# Complex flow and reflection of evanescent waves from a nanometer-sized hole in a cylindrical waveguide

T. I. Kuznetsova* and V. S. Lebedev
*P.N. Lebedev Physical Institute, Leninsky prospect 53, Moscow 119991, Russia*
*and Moscow Institute of Physics and Technology (State University), Institutskiĭ per., 9, Dolgoprudnyĭ, Moscow Oblast, 141700, Russia*

(Received 8 October 2007; revised manuscript received 23 April 2008; published 31 July 2008)

The results of the theoretical studies on the leakage of the optical radiation through a truncated waveguide with a subwavelength-sized exit hole are reported. We develop a self-consistent approach for the description of the fields behavior by taking into account the transformation of the initial wave into all possible modes, which appear due to the influence of the exit aperture. Our approach allows us to evaluate the amplitude reflection coefficient for the initial evanescent wave and to establish its relationship with the impedance of an infinite waveguide and the impedance of the exit aperture coupling a truncated waveguide with a free space. We determine the complex flow through the exit hole and the transmission coefficient to the far-field zone and express them through the reflection coefficient. Special attention in the work is paid to the evaluation of specific dependencies of the reflection and transmission coefficients on the ratio of the aperture radius to the light wavelength, on the dielectric constants of the waveguide core and the surrounding matter, and on the type of the waveguide mode. It is demonstrated that in the case of a metallic matter at the exit of a waveguide there is a strong resonance enhancement in the amplitude of the reflected wave and in the resulting amplitude of the tangential component of the electric field.

DOI: 10.1103/PhysRevE.78.016607 PACS number(s): 41.20.−q, 42.25.Bs, 42.25.Fx

## I. INTRODUCTION

Modern studies of the optical properties of nanoscale structures are based on the utilization of light fields localized on the subwavelength dimensions [1]. There is now a number of efficient methods for the creation of strongly localized optical fields. A considerable part of them is based on the transformation of the optical radiation into the subwavelength-sized electromagnetic fields using the aperture-type near-field optical probes [2–4], single subwavelength hole [5,6] or slit, and the periodic hole arrays [7,8] in a metallic screen.

An evident advance has been achieved to date in the theoretical description of light transmission through the aperture-type near-field optical probes tapered to a subwavelength diameter. For example, there is a number of calculations [9,10] of light transmission through the near-field optical fiber tips with a metal coating made with the use of the multiple multipole method. The two-dimensional model, based on the Lippman-Schwinger formalism, has been developed in [11,12]. Theoretical treatment of the optical transmission through the metal-coated near-field probes, based on the consideration of the eigenmodes in a conical waveguide, was given in a series of our papers for the cases of the dielectric [13,14] and semiconducting [15–18] core. Finite-difference time-domain simulation for the optimization of the fiber tip parameters was employed in [19–21].

In the case of a single subwavelength-sized circular aperture in a perfectly conducting metallic screen, the basic theoretical aspects of light transmission to the near-field and to the far-field zones have been formulated in the classical papers by Bethe and Bouwkamp [22,23]. These authors have obtained a rigorous solution for the electromagnetic fields by using the static solutions for the near field existing in the vicinity of the hole. The final results of the theory [22,23] for the transmission coefficient to the far-field zone are in agreement with those previously obtained by Rayleigh [24] in his diffraction theory of electromagnetic radiation by small particles (see [25]).

Further, a consideration of the electromagnetic wave, which impinges from a free space onto the open end of a waveguide with perfectly conducting walls, was performed in [26]. Light diffraction through a subwavelength-sized aperture located at the apex of a metallic screen with conical geometry was considered in [27]. Numerical calculations of light transmission through a subwavelength circular hole in a metallic film were made in [28–33] by taking into account the finite thickness of a channel and its dielectric properties. It was demonstrated that transmission efficiency of light through such a hole can be significantly enhanced if a channel in the film is filled by a material of sufficiently high permittivity. A suggested mechanism of such enhancement in a single hole consists of the presence of a cavity mode that couples resonantly to the incident light.

In the last decade a series of interesting theoretical works has been devoted to the description of some unusual plasmon-supported effects observed in light transmission through a single subwavelength hole or the hole arrays in metallic films (see [34,35] and references therein). Here we mean, first of all, the works [36–38] on highly directional emission from a single subwavelength aperture surrounded by periodic surface corrugations as well as a series of papers [39–43] on the plasmon-supported extraordinary transmission through periodic subwavelength-sized hole arrays in thin metallic films. Surface plasmon generation and light

*tkuzn@sci.lebedev.ru

 

transmission by a single isolated nanohole in thin and thick metal films were studied in Refs. [44–48]. It was shown that elastic scattering spectra from the nanoholes in noble metal films exhibit a broad resonance in the long-wavelength part of the visible spectrum leading to enhancing transmission of light through an isolated aperture.

In many cases of practical importance, however, the relative influence of the plasmon-supported phenomena and diffraction effects on the behavior of light reflection and transmission through a subwavelength hole of a metal-coated waveguide remains unclear. It is strongly dependent on the wavelength, the aperture diameter, specific value of a complex dielectric function of a metallic cladding, as well as on the permittivity of a waveguide core and a surrounding matter. Definitely, however, there is a number of problems associated with the field transformation from the supercritical waveguide or the near-field probe to a surrounding matter, which need additional studies but are not directly connected with the consideration of the plasmon-supported effects in a metallic coating of the probe.

In this work we develop a theoretical approach for the description of the evanescent field behavior inside a truncated waveguide. The approach is based on a self-consistent technique for matching the fields at an interface between a free space and a waveguide. Here it is important to note that there is a series of works by Vaynshteyn (see [49,50]) devoted to the studies of the electromagnetic fields in the truncated waveguides. However, in contrast to the case of the evanescent waves, his theory is related to the case of the propagating waves. So, it cannot be directly applied for the description of supercritical waveguides, which are of special interest for the near-field optics. Here we elaborate on a theory for the description of the transmission and the reflection of the evanescent waves from a nanometric hole in a metal-coated waveguide. Our technique allows us to evaluate the field perturbances, which appear at the exit aperture of a waveguide, and to establish the relationships between the amplitude reflection coefficient, the complex flow, and the electric field square integrated over the aperture. On the basis of the results obtained we study the effects, associated with the jump in the dielectric function at the boundary of a waveguide and a surrounding matter, and discuss their influence on the reflection coefficient.

A consideration of the aforementioned problems is performed in the present work for the case of a cylindrical geometry of a supercritical waveguide. Note also that we concentrate on a study of a mechanism of light transmission at which the energy is primarily transported by the waves inside a core of a waveguide. So, throughout the paper we consider a cylindrical waveguide with perfectly conducting metallic walls. Some specific calculations of the field characteristics for a waveguide with a finite reflectivity of its metallic walls will be performed only at the end of Sec. III, where we briefly outline a way for the extension of our approach to the case of a real metal and present some results for an Al cladding at $\lambda=488$ nm. A consideration of the plasmon-supported phenomena similar to those observed in noble metal films (see [35], and references therein) is outside the scope of the present work. We restrict our consideration to the case of the lowest-order transverse-magnetic, $TM_{01}$, mode. At the end of the paper, we outline a technique for the description of the angular-symmetrical transverse-electric, $TE_{01}$, mode.

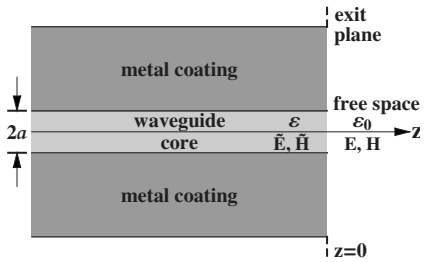


FIG. 1. Transverse section of a metal-coated cylindrical waveguide: $2a$ is the aperture diameter, $\varepsilon$ and $\varepsilon_0$ are the dielectric constants of the waveguide core and a surrounding matter, respectively.

## II. CONSIDERATION OF THE EVANESCENT AND GUIDING TRANSVERSE-MAGNETIC, $TM_{01}$, WAVES

### A. Fields behavior inside an infinite waveguide

In this section we present the basic formulas for the monochromatic electromagnetic field in a circular cylindrical waveguide (see Fig. 1). We omit further the time-oscillating factor $\exp(-i\omega t)$ from all expressions and we use the cylindrical coordinates $\rho$, $\varphi$, and $z$. The basic formulas for the transverse-magnetic, $TM_{mn}$, and transverse-electric, $TE_{mn}$, field modes inside a cylindrical waveguide with perfectly conducting metallic walls are presented in Refs. [50,51]. In the present paper we consider the transverse-magnetic modes $TM_{0n}$ with azimuthal wave number $m=0$. In this case there are only three nonzero field components, $\tilde{E}_\rho$, $\tilde{E}_z$, and $\tilde{H}_\varphi$, which are independent on $\varphi$. The basic formulas for the field components can be written in terms of the Bessel function of zero index $J_0(x)$ and its derivative $J_1(x)$:

$$\tilde{E}_\rho = CJ_1(q\rho)\exp\left(-z\sqrt{q^2-\frac{\omega^2\varepsilon}{c^2}}\right), \tag{1}$$

$$\tilde{E}_z = \frac{q}{\sqrt{q^2-\frac{\omega^2\varepsilon}{c^2}}}CJ_0(q\rho)\exp\left(-z\sqrt{q^2-\frac{\omega^2\varepsilon}{c^2}}\right), \tag{2}$$

$$\tilde{H}_\varphi = -\frac{i\omega\varepsilon}{c}\frac{1}{\sqrt{q^2-\frac{\omega^2\varepsilon}{c^2}}}CJ_1(q\rho)\exp\left(-z\sqrt{q^2-\frac{\omega^2\varepsilon}{c^2}}\right). \tag{3}$$

Here $q\equiv q_{0n}=\xi_{0n}/a$ is the transverse wave number, $\xi_{0n}$ is the $n$th zero of the Bessel function $J_0(x)$ ($\xi_{01}=2.4048$, $\xi_{02}=5.5201$, $\xi_{03}=8.6537,\ldots$), $a$ is the waveguide radius, $C$ is a constant, and $\varepsilon$ is the dielectric constant of the waveguide core. Further we omit the first index, $m=0$, and write $q_1$, $q_2$, $q_3,\ldots$ and $\xi_1$, $\xi_2$, $\xi_3,\ldots$ in all expressions presented below.

### B. Fourier-Bessel expansion of the field components in a free space

In a free space ($z>0$, see Fig. 1) for the field components there is a continuous set of the transverse wave numbers, $\varkappa$,

in contrast to the case of a waveguide with a discrete set of eigenmodes. Then, the field components can be expressed as the Fourier-Bessel integral taken over the transverse wave number

$$E_\rho = \int_0^\infty \exp\left( iz\sqrt{\frac{\omega^2\varepsilon_0}{c^2} - \varkappa^2}\right) J_1(\varkappa\rho)B(\varkappa)\varkappa d\varkappa, \quad (4)$$

$$E_z = i\int_0^\infty \exp\left( iz\sqrt{\frac{\omega^2\varepsilon_0}{c^2} - \varkappa^2}\right) \frac{\varkappa J_0(\varkappa\rho)B(\varkappa)\varkappa d\varkappa}{\sqrt{\frac{\omega^2\varepsilon_0}{c^2} - \varkappa^2}}, \quad (5)$$

$$H_\varphi = \frac{\omega\varepsilon_0}{c}\int_0^\infty \exp\left( iz\sqrt{\frac{\omega^2\varepsilon_0}{c^2} - \varkappa^2}\right) \frac{J_1(\varkappa\rho)B(\varkappa)\varkappa d\varkappa}{\sqrt{\frac{\omega^2\varepsilon_0}{c^2} - \varkappa^2}}. \quad (6)$$

Here $B(\varkappa)$ is the expansion coefficient, and $\varepsilon_0$ is the dielectric constant of the free space. To simplify the formulas, we suppose it to be real throughout the present paper. On the condition that $\varkappa^2 > \omega^2\varepsilon_0/c^2$, the square root $\sqrt{\omega^2\varepsilon_0/c^2 - \varkappa^2}$ in Eqs. (4)–(6) should be replaced by $i\sqrt{\varkappa^2 - \omega^2\varepsilon_0/c^2}$. This replacement corresponds to the description of the evanescent waves instead of the guiding waves. Note also that the specific form of these expressions is determined by the requirement that the propagation of the electromagnetic wave (or its decay) is permitted only in the positive $z$ direction and is forbidden in the opposite direction.

### C. Description of the evanescent waves in a truncated cylindrical waveguide

#### 1. General formulas

We consider now a waveguide which is truncated at some plane, $z=0$ (see Fig. 1). Our aim is to study the influence of the exit hole located at $z=0$ on the field behavior. The influence of the entrance hole will be neglected since the interference effects from the two holes cannot be important in the case of the evanescent waves if the total length of a waveguide exceeds the attenuation length of the field in the core matter. Besides, we suppose that the influence of such factors as the transmission coefficient of the entrance hole and the field decay along the waveguide length has already been taken into account by an appropriate choice of the $C$ constant in Eqs. (1)–(3). So, we concentrate here on the studies of the field transformations at the exit plane.

To get a self-consistent description of the field behavior at the exit plane we have to match the fields related to the waveguide with those related to the free space. To this end, we must equalize both the $E_\rho$ and $H_\varphi$ components at the waveguide exit, i.e., to put $\tilde{E}_\rho = E_\rho$ and $\tilde{H}_\varphi = H_\varphi$ at $z=0$, $\rho < a$. In addition, below we assume that the waveguide exit is adjoined to a perfectly conducting metallic flange extending from $\rho=a$ to $\rho=\infty$. So, we put $E_\rho=0$ at the outer surface of the flange. It is also important to stress that for matching the fields at the waveguide exit aperture ($z=0$) by the relevant way, we must take into account all possible transverse-magnetic waveguide modes and to incorporate them into the basic expressions (1)–(3). As a result, we obtain the following expressions for the electric field components inside a truncated waveguide:

$$\tilde{E}_\rho = C\left\{ J_1(q_1\rho)\exp\left( -z\sqrt{q_1^2 - \frac{\omega^2\varepsilon}{c^2}}\right) + \sum_{n=1}^\infty \alpha_n J_1(q_n\rho)\exp\left( z\sqrt{q_n^2 - \frac{\omega^2\varepsilon}{c^2}}\right)\right\}, \quad (7)$$

$$\tilde{E}_z = C\left\{ \frac{q_1 J_0(q_1\rho)}{\sqrt{q_1^2 - \omega^2\varepsilon/c^2}}\exp\left( -z\sqrt{q_1^2 - \frac{\omega^2\varepsilon}{c^2}}\right) - \sum_{n=1}^\infty \alpha_n \frac{q_n J_0(q_n\rho)}{\sqrt{q_n^2 - \omega^2\varepsilon/c^2}}\exp\left( z\sqrt{q_n^2 - \frac{\omega^2\varepsilon}{c^2}}\right)\right\} \quad (8)$$

instead of Eqs. (1) and (2). Similarly, the nonzero component of the magnetic field inside a waveguide can be written as

$$\tilde{H}_\varphi = -i\frac{\omega}{c}\varepsilon C\left\{ \frac{J_1(q_1\rho)}{\sqrt{q_1^2 - \omega^2\varepsilon/c^2}}\exp\left( -z\sqrt{q_1^2 - \frac{\omega^2\varepsilon}{c^2}}\right) - \sum_{n=1}^\infty \frac{\alpha_n J_1(q_n\rho)}{\sqrt{q_n^2 - \omega^2\varepsilon/c^2}}\exp\left( z\sqrt{q_n^2 - \frac{\omega^2\varepsilon}{c^2}}\right)\right\}. \quad (9)$$

The basic expressions for the fields outside a waveguide remain the same as in the preceding section.

#### 2. Electromagnetic fields at the waveguide exit

Starting from Eqs. (7)–(9) for the fields inside a waveguide, we obtain the required expressions for the field components at the waveguide exit ($z=0$),

$$\tilde{E}_\rho(\rho,z)|_{z=0} = C\sum_{n=1}^\infty (\delta_{n1} + \alpha_n)J_1(q_n\rho), \quad (10)$$

$$\tilde{E}_z(\rho,z)|_{z=0} = C\left\{ \sum_{n=1}^\infty \frac{(\delta_{n1} - \alpha_n)q_n J_0(q_n\rho)}{\sqrt{q_n^2 - \omega^2\varepsilon/c^2}}\right\}, \quad (11)$$

$$\tilde{H}_\varphi(\rho,z)|_{z=0} = -iC\left(\frac{\omega\varepsilon}{c}\right)\left\{ \sum_{n=1}^\infty \frac{(\delta_{n1} - \alpha_n)}{\sqrt{q_n^2 - \frac{\omega^2\varepsilon}{c^2}}}J_1(q_n\rho)\right\}, \quad (12)$$

where $\delta_{pq}$ is the Kronecker delta.

Similarly, starting from the basic equations for the field components, related to a free space, we have

$$E_\rho(\rho,z)|_{z=0} = \int_0^\infty J_1(\varkappa\rho)B(\varkappa)\varkappa d\varkappa, \quad (13)$$

$$E_z(\rho,z)|_{z=0} = \int_0^\infty \varkappa J_0(\varkappa\rho)B(\varkappa)\frac{\varkappa d\varkappa}{\gamma(\varkappa)}, \quad (14)$$

$$H_\varphi(\rho,z)|_{z=0} = -i\frac{\omega\varepsilon_0}{c}\int_0^\infty J_1(\varkappa\rho)B(\varkappa)\frac{\varkappa d\varkappa}{\gamma(\varkappa)}. \quad (15)$$

Here the following notation is to be introduced:

$$\gamma(\varkappa)=\begin{cases}-i\sqrt{\omega^2\varepsilon_0/c^2-\varkappa^2} & (\omega^2\varepsilon_0/c^2>\varkappa^2),\\ \sqrt{\varkappa^2-\omega^2\varepsilon_0/c^2} & (\omega^2\varepsilon_0/c^2\le\varkappa^2).\end{cases} \tag{16}$$

## III. REFLECTION COEFFICIENT

### A. Matching the fields at an interface of a waveguide and a free space

For the transverse-magnetic mode, $TM_{0n}$, the boundary conditions at an interface ($z=0$) of a waveguide and a free space have the form

$$E_\rho(\rho,0)=\tilde{E}_\rho(\rho,0),$$

$$H_\varphi(\rho,0)=\tilde{H}_\varphi(\rho,0). \tag{17}$$

We insert now expressions (10) and (13) for $\tilde{E}_\rho(\rho,0)$ and $E_\rho(\rho,0)$ into the first boundary condition (17) and use the following formula for the Bessel function:

$$J_1(q_n\rho)\,\theta(a-\rho)=\int_0^\infty b_n(\varkappa)J_1(\varkappa\rho)\varkappa d\varkappa, \tag{18}$$

where the $b_n$ coefficients are defined by the relation

$$b_n(\varkappa)=\int_0^a J_1(q_n\rho)J_1(\varkappa\rho)\rho d\rho=J_1(q_na)\frac{\varkappa aJ_0(\varkappa a)}{q_n^2-\varkappa^2}. \tag{19}$$

Here $q_na=\xi_n$ are the Bessel zeros $J_0(\xi_n)=0$, and $\theta(a-\rho)$ is the Heaviside step function [i.e., $\theta(a-\rho)=0$ when $a<\rho$, and $\theta(a-\rho)=1$ when $\rho\le a$]. As a result, the first boundary condition for $E_\rho$ leads to the following expression for the Fourier-Bessel coefficients:

$$B(\varkappa)=C\sum_{n=1}^{\infty}(\delta_{n1}+\alpha_n)b_n(\varkappa). \tag{20}$$

Further we can rewrite Eq. (15) for the $H_\varphi$ component in a free space as

$$H_\varphi(\rho,0)=-i\frac{\omega\varepsilon_0}{c}C\int_0^\infty\frac{1}{\gamma(\varkappa)}\sum_{n=1}^{\infty}(\delta_{n1}+\alpha_n)b_n(\varkappa)J_1(\varkappa\rho)\varkappa d\varkappa. \tag{21}$$

On inserting this expression into the second boundary condition for $H_\varphi$, we get

$$\varepsilon\sum_{n=1}^{\infty}\frac{(\delta_{n1}-\alpha_n)}{\sqrt{q_n^2-\frac{\omega^2\varepsilon}{c^2}}}J_1(q_n\rho)=\varepsilon_0\int_0^\infty\frac{1}{\gamma(\varkappa)}\sum_{n=1}^{\infty}(\delta_{n1}+\alpha_n)b_n(\varkappa)J_1(\varkappa\rho)\varkappa d\varkappa. \tag{22}$$

The next step consists of the multiplication of both sides of Eq. (22) by a factor $J_1(q_p\rho)$ and in the integration of the resulting expression over the $\rho d\rho$ within the limits from 0 to $a$. Note that for the unequal magnitudes of $n$ and $p$ the Bessel functions are orthogonal because they are the eigenfunctions of the boundary-value problem of the third kind (they obey the Bessel equation and the following boundary condition $\partial J_1/\partial\rho+a^{-1}J_1=0$ at $\rho=a$). Therefore upon integration over the $\rho d\rho$ we obtain

$$\varepsilon\frac{(\delta_{p1}-\alpha_p)}{\sqrt{q_p^2-\frac{\omega^2\varepsilon}{c^2}}}\int_0^a J_1^2(q_p\rho)\rho d\rho=\varepsilon_0\sum_{n=1}^{\infty}(\delta_{n1}+\alpha_n)\int_0^a J_1(q_p\rho)\rho d\rho\int_0^\infty b_n(\varkappa)J_1(\varkappa\rho)\frac{\varkappa d\varkappa}{\gamma(\varkappa)}. \tag{23}$$

Then, we change the order of integration in the right-hand side of this equation and use Eq. (19) for the $b_n$ coefficient as well as the following relation for the integral in the left-hand side of Eq. (23):

$$\int_0^a J_1^2(q_n\rho)\rho d\rho=\frac{a^2}{2}J_1^2(q_na), \tag{24}$$

which is true when $J_0(q_na)=0$.

As a result, we derive a rigorous system of equations for the determination of the amplitude reflection coefficients, $\alpha_p$, of the evanescent modes associated with the transformation of the initial $TM_{01}$ wave

$$\varepsilon\frac{(\delta_{p1}-\alpha_p)}{\sqrt{q_p^2a^2-\varepsilon\frac{\omega^2}{c^2}a^2}}=2\varepsilon_0\sum_{n=1}^{\infty}(\delta_{n1}+\alpha_n)\frac{J_1(q_na)}{J_1(q_pa)}I_{np}. \tag{25}$$

The real and imaginary parts of the integral $I_{np}=\mathrm{Re}\{I_{np}\}+i\,\mathrm{Im}\{I_{np}\}$ in Eq. (25) are given by

$$\mathrm{Re}\{I_{np}\}=\int_{\omega a/c\sqrt{\varepsilon_0}}^\infty\frac{[xJ_0(x)]^2}{(q_n^2a^2-x^2)(q_p^2a^2-x^2)}\frac{xdx}{\sqrt{x^2-\frac{\omega^2\varepsilon_0}{c^2}a^2}}, \tag{26}$$

$$\mathrm{Im}\{I_{np}\}=\int_0^{\omega a/c\sqrt{\varepsilon_0}}\frac{[xJ_0(x)]^2}{(q_n^2a^2-x^2)(q_p^2a^2-x^2)}\frac{xdx}{\sqrt{\frac{\omega^2\varepsilon_0}{c^2}a^2-x^2}}. \tag{27}$$

The quantities (26) and (27) play the key role in the evaluation of the reflection and the transmission properties of the evanescent and guiding waves in a waveguide with a subwavelength exit hole. We discuss below their behavior as functions of the $ka$ value, where $k=\omega\sqrt{\varepsilon_0}/c$ is the wave number in a free space. First, we note that at $ka\ll1$, the absolute values of the integrals $I_{np}$ satisfy the relation $|I_{np}|\ll|I_{nn}|$ at $n\neq p$. The imaginary part of the integral $I_{np}$ is considerably less than the modulus of its real part. Its asymptotic expression at $n=p$ takes the form

$$\mathrm{Im}\{I_{nn}\}=\frac{2}{3\xi_n^4}(ka)^3\quad(ka\ll1), \tag{28}$$

so that $\mathrm{Im}\{I_{nn}\}=0$ at $ka=0$. In addition, the absolute value of the integral $I_{np}$ at $n=p$ can be roughly estimated as

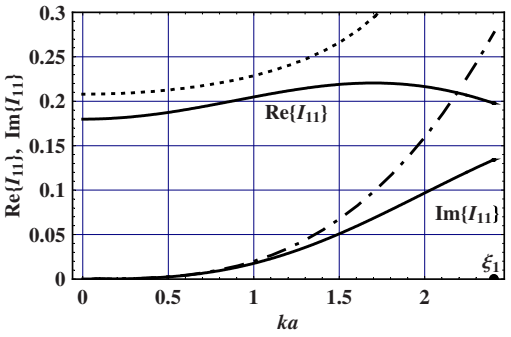


FIG. 2. (Color online) Real and imaginary parts of the integral $I_{11}$ vs $ka$ ($k=\omega\sqrt{\varepsilon_0}/c$). The full curves are the results obtained using the basic equations (26) and (27). The dashed-dotted curve represents calculations by the asymptotic formula (28) at $n=1$. The dotted curve is the rough estimate of $|I_{11}|$ [see Eq. (29)].

$$|I_{nn}| \approx \frac{1}{2\sqrt{q_n^2 a^2 - \omega^2 a^2 \varepsilon_0 / c^2}}. \tag{29}$$

In Fig. 2 we present the results of exact calculations of Re$\{I_{11}\}$and Im$\{I_{11}\}$ obtained using the basic formulas (26) and (27). It is seen that the value of Re$\{I_{11}\}$ slightly varies in the whole range of $ka$ under consideration ($0 \le ka \le \xi_1$). The imaginary part of the integral $I_{11}$ strongly grows with an increase of the $ka$ value.

### B. First-order approximation

As a first-order approximation to the solution of the system (25) we take the solution for which all nondiagonal coefficients, $I_{np}$ $(n \neq p)$, are equal to zero. This yields

$$\frac{(1-\alpha_1)\varepsilon}{\sqrt{q_1^2 a^2 - \frac{\omega^2 a^2 \varepsilon}{c^2}}} = 2\varepsilon_0(1+\alpha_1)I_{11}, \tag{30}$$

$$-\frac{\alpha_p \varepsilon}{\sqrt{q_p^2 a^2 - \frac{\omega^2 a^2 \varepsilon}{c^2}}} = 2\varepsilon_0 \alpha_p I_{pp}. \tag{31}$$

Hence the amplitude reflection coefficient, $\alpha_1$, in the first-order approximation has the form

$$\alpha_1^{(1)} = \frac{1 - G^{(1)}}{1 + G^{(1)}},$$

$$G^{(1)} = 2\left(\frac{\varepsilon_0}{\varepsilon}\right) I_{11} \sqrt{q_1^2 a^2 - \frac{\omega^2 a^2 \varepsilon}{c^2}}, \tag{32}$$

while all other coefficients are equal to zero,

$$\alpha_n^{(1)} = 0 \quad (n \neq 1). \tag{33}$$

Formula (32) allows us to obtain a simple asymptotic expression for the reflection coefficient at small values of the $a/\lambda$ ratio. In particular, at $\varepsilon = \varepsilon_0 = 1$ we get

$$\mathrm{Re}\{\alpha_1\} = 0.0724,$$

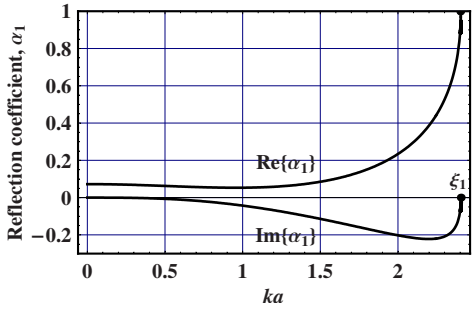


FIG. 3. (Color online) The amplitude reflection coefficient, $\alpha_1$, as a function of $ka$ ($k=\omega\sqrt{\varepsilon_0}/c$). Calculations were made within the framework of the first-order approximation (32) for the $TM_{01}$ mode in a hollow waveguide ($\varepsilon=1$). The dielectric constant of a free space, $\varepsilon_0$, was taken to be equal to unity.

$$\mathrm{Im}\{\alpha_1\} = -0.0551(ka)^3. \tag{34}$$

The specific shape of the amplitude reflection coefficient, $\alpha_1$, in a wide range of $ka$ $(0 \le ka \le \xi_1)$ is shown in Fig. 3. It is seen that its real part is slightly dependent on the $a/\lambda$ ratio in all of the subwavelength range, including the magnitudes of $ka \sim 1$. Its strong increase occurs only starting from $ka \approx 1.5$ as this value approaches the eigenvalue, $\xi_1 = q_1 a$, of the $TM_{01}$ mode. On the contrary, the imaginary part of $\alpha_1$ strongly falls with an increase of $ka$ straight away from 0, reaches its minimum at $ka=2.2$, then strongly grows and vanishes at $ka=\xi_1$.

To clarify the physical meaning of the coefficient, $\alpha_1$, we should take into account that it gives the transformation coefficient of the initial evanescent $TM_{01}$ mode into the "reflected mode" (rigorously speaking, into the mode with the same transverse structure and the inverted $z$ dependence). Note that the $\alpha_1$ coefficient is a complex value, whose real part is much greater than the modulus of the imaginary part $(\mathrm{Re}\{\alpha_1\} \gg \mathrm{Im}\{-\alpha_1\}$, see Fig. 3).

In the near-field zone (including the region at the waveguide exit, $z=0$) the field strength and the energy density are primarily determined by the real part of the $\alpha_1$ coefficient. In particular, the value of $\mathrm{Re}\{\alpha_1\} \approx 1$ corresponds to the loop of the transverse component, $E_\rho$, of the electric field at the waveguide exit ($z=0$) and, respectively, to the node for the $E_z$ and $H_\varphi$ components [see Eqs. (10)–(12)]. On the contrary, the value of $\mathrm{Re}\{\alpha_1\} \approx -1$ corresponds to the loop of the $H_\varphi$ and $E_z$ components and to the node of the $E_\rho$ component. The real part of $\alpha_1$ is not responsible for the energy flux. The imaginary part of the amplitude reflection coefficient, $\mathrm{Im}\{\alpha_1\}$, is directly connected with the energy flux, and, correspondingly, with the transmission coefficient to the far-field zone (see Secs. IV and V). Hence the energy flux does not equal zero only on the condition that $\mathrm{Im}\{\alpha_1\} \neq 0$, which is true if $\mathrm{Im}\{I_{11}\} \neq 0$. The strong difference between the values of Re$\{\alpha_1\}$ and Im$\{\alpha_1\}$ enables us to demonstrate the important quantitative differences between the field strengths in the near-field and in the far-field zones.

### C. Second-order approximation

In the second-order approximation the basic system of equations for the amplitude reflection coefficients, $\alpha_p$, is reduced to the form

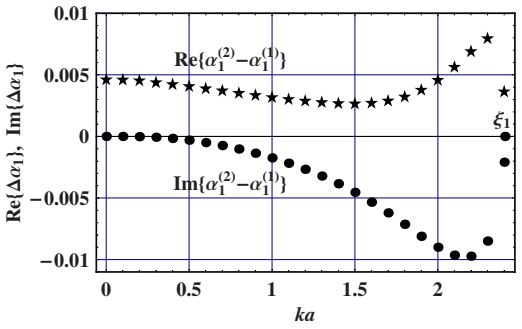


FIG. 4. (Color online) Differences between the results of calculations of the real (stars) and imaginary (circles) parts of the amplitude reflection coefficient, $\alpha_1$, obtained in the second-order and in the first-order approximations. Calculations were made for a hollow waveguide ($\varepsilon=1$). The dielectric constant of a free space, $\varepsilon_0$, was taken to be equal to unity.

$$-\alpha_p\left(\frac{\varepsilon}{\sqrt{q_p^2a^2-\omega^2a^2\varepsilon/c^2}}+2\varepsilon_0 I_{pp}\right)=2\varepsilon_0(1+\alpha_1)\frac{J_1(q_1a)}{J_1(q_pa)}I_{1p},$$
$$p\neq 1 \tag{35}$$

$$(1-\alpha_1)\frac{\varepsilon}{\sqrt{q_1^2a^2-\omega^2a^2\varepsilon/c^2}}-2\varepsilon_0(1+\alpha_1)I_{11}$$
$$=2\varepsilon_0\sum_{n=2}^{\infty}\alpha_n\frac{J_1(q_na)}{J_1(q_1a)}I_{n1}. \tag{36}$$

The solution of this system leads to the following expression for the amplitude reflection coefficient $\alpha_1$, associated with the $TM_{01}$ mode:

$$\alpha_1^{(2)}=\frac{1-G^{(2)}}{1+G^{(2)}},$$

$$G^{(2)}=G^{(1)}-\frac{4\varepsilon_0}{\varepsilon}\sqrt{(q_1a)^2-\omega^2a^2\varepsilon/c^2}$$
$$\times\sum_{n=2}^{\infty}\frac{I_{1n}I_{n1}}{\left(2I_{nn}+\frac{\varepsilon/\varepsilon_0}{\sqrt{(q_na)^2-\omega^2a^2\varepsilon/c^2}}\right)}. \tag{37}$$

The reflection coefficients for the higher-order $TM_{0n}$ modes ($n=2,3,4,\ldots$) are given by

$$\alpha_n^{(2)}=-\frac{2I_{1n}(1+\alpha_1^{(2)})}{\left(2I_{nn}+\frac{\varepsilon/\varepsilon_0}{\sqrt{(q_na)^2-\omega^2a^2\varepsilon/c^2}}\right)}\frac{J_1(q_1a)}{J_1(q_na)}. \tag{38}$$

Our analysis clearly demonstrates that the second-order approximation gives small corrections to the results for $\alpha_1$ obtained previously in the first-order approximation. This is directly evident from Fig. 4, where we display the real (stars) and imaginary (circles) parts of the differences between the $\alpha_1$ coefficients, calculated in the second-order and in the first-order approximations for a hollow waveguide. The calculations were made by Eqs. (32) and (37) in a wide range of the ratio of the aperture radius to the light wavelength ($0\leq ka\leq\xi_1=2.4048$). It is seen that the relative errors in the evaluation of the real, $(\mathrm{Re}\{\alpha_1^{(2)}\}-\mathrm{Re}\{\alpha_1^{(1)}\})/\mathrm{Re}\{\alpha_1^{(2)}\}$, and imaginary, $(\mathrm{Im}\{\alpha_1^{(2)}\}-\mathrm{Im}\{\alpha_1^{(1)}\})/\mathrm{Im}\{\alpha_1^{(2)}\}$, parts of the reflection coefficient in the first-order approximations do not exceed 6% and 5%, respectively.

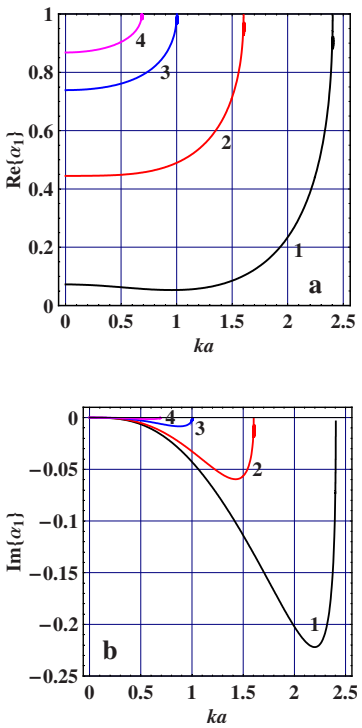


FIG. 5. (Color online) Real (a) and imaginary (b) parts of the amplitude reflection coefficient, $\alpha_1$, vs $ka$ ($k=\omega\sqrt{\varepsilon_0}/c$). Curves 1–4 correspond to various values of the refractive indices ratio $\sqrt{\varepsilon/\varepsilon_0}=1$, 1.5, 2.4, and 3.5, respectively.

It is important to stress that independently of the specific values of the $\alpha_n$ coefficients (corresponding to the higher-order modes $n=2,3,4,\ldots$) they cannot affect the magnitude of the energy flux through the exit aperture, associated with the initial $TM_{01}$ mode. Indeed, the evanescent mode should bear the flux only being combined with the same mode of the inverted axial direction.

### D. Dependencies of the reflection coefficient on the dielectric constants and the $a/\lambda$ ratio

We consider now the behavior of the amplitude reflection coefficient in dependence on the dielectric constants of a waveguide core, $\varepsilon$, and a surrounding matter, $\varepsilon_0$, as well as on the ratio of the aperture diameter to the radiation wavelength. To this end, we present in Fig. 5 the results of our calculations of $\mathrm{Re}\{\alpha_1\}$ and $\mathrm{Im}\{\alpha_1\}$ for several typical cases, in which the dielectric constant of a free space outside a waveguide is equal to $\varepsilon_0=1$, while the values of the refractive index, $n=\sqrt{\varepsilon}$, of the waveguide core are 1.5, 2.4, and 3.5 (curves 2, 3, and 4 in Fig. 5). This corresponds to the dielectric constants of the fiber, silicon nitride, and semiconducting (e.g., Si) core. So, the obtained results are of interest for the applications to the near-field optical probes.

It is seen that all general features in the dependencies of the real and imaginary parts of the amplitude reflection co-

efficient as functions of the $ka$ value remain the same as in the case of a hollow waveguide (curves 1 in Fig. 5). However, the specific values of $\mathrm{Re}\{\alpha_1\}$ and $\mathrm{Im}\{\alpha_1\}$ differ substantially from the discussed above case of $\varepsilon=\varepsilon_0$. In other words, they are considerably dependent on the magnitude of the $\varepsilon/\varepsilon_0$ ratio. As follows from the comparison of curves 1–4 in Fig. 5(a), for a given magnitude of $ka$, the value of $\mathrm{Re}\{\alpha_1\}$ strongly increases with a growth of the $\varepsilon/\varepsilon_0$ ratio. In particular, for the waveguides with the fiber, silicon nitride, and silicon core the real part of the amplitude reflection coefficient at small $ka$ magnitudes exceeds the corresponding value for a hollow waveguide for approximately 6.1, 10.2, and 12.0 times, respectively. Note also that the positions of the $ka$ points, at which the value of $\mathrm{Re}\{\alpha_1\}$ becomes equal to unity and $\mathrm{Im}\{\alpha_1\}$ vanishes [see Fig. 5(b)], are determined by the relation $ka=\xi_1\sqrt{\varepsilon_0/\varepsilon}$, where $\xi_1=q_1a=2.4048$.

Here it is worthwhile to remember that the real part of the $\alpha_1$ coefficient is not related to the reflection of the energy flux. An increase of the $\mathrm{Re}\{\alpha_1\}$ value means a growth of the energy density of the electric field component, $E_\rho$, in the near-field zone. As is evident from Fig. 5(a), the value of $\mathrm{Re}\{\alpha_1\}$ becomes close to unity at large values of $\varepsilon/\varepsilon_0$. Such an effect differently affects the values of the energy densities, associated with different field components at the waveguide exit. Whereas the energy density $w_\rho\propto|1+\alpha_1|^2$ (associated with the transverse component of the electric field, $E_\rho$) can be approximately four times greater than that for the unperturbed waveguide of an infinite length, the energy densities $w_\varphi, w_z\propto|1-\alpha_1|^2$ of the magnetic field, $H_\varphi$, and the longitudinal component of the electric field, $E_z$, tend to zero at $\alpha_1\to 1$. Thus for the dominant (at $ka\ll 1$) contribution, $w_\rho$, to the energy density, this effect acts in the same direction as an effect, associated with a decrease of the evanescent wave damping in the supercritical waveguide at a large dielectric constant of its core.

Further, we additionally clarify the role of a jump in the dielectric constants at an interface between a waveguide and a surrounding matter. To this end, we display the amplitude reflection coefficient as a function of the $\varepsilon_0/\varepsilon$ ratio for a fixed positive value of the waveguide dielectric constant, $\varepsilon$, and a given value of $\omega a\sqrt{\varepsilon}/c=\pi/5$ (see Fig. 6). It is seen that the behavior of the reflection coefficient, $\alpha_1$, turns out to be quite different for the positive and negative dielectric constants of a surrounding matter, $\varepsilon_0$. From the physical point of view, the negative values of the $\varepsilon_0/\varepsilon$ ratio correspond to the case of a metallic medium outside a waveguide and a fixed positive value of the core dielectric constant (e.g., a waveguide with the fiber core). One should remember that the real part of the $\alpha_1$ coefficient is not related with the energy flux. An increase of the $\mathrm{Re}\{\alpha_1\}$ value means an increase of the energy density of the electric field component, $E_\rho$, in the near-field zone. As is evident from Fig. 6(a), the value of $\mathrm{Re}\{\alpha_1\}$ becomes close to unity at large values of the $\varepsilon_0/\varepsilon$ ratio. The interesting features in the behavior of $\alpha_1$ appear when the $\varepsilon_0/\varepsilon$ ratio reaches some definite value $-1.274$. Such a singularity in the dependence of $\mathrm{Re}\{\alpha_1\}$ on $\varepsilon_0/\varepsilon$ actually reflects a strong increase in the amplitude of the reflected wave [and, hence, in the resulting value of the transverse component of the electric field $E_\rho\propto(1+\alpha_1)$]. For the waveguide with the fiber core ($n=\sqrt{\varepsilon}=1.5$) this increase occurs at the magnitude of the dielectric constant of external matter equal to $\varepsilon_0=-2.866$. Taking into account the behavior of the dielectric functions of silver and gold on light wavelength in vacuum (see [52]), we obtain that for the Ag and Au substrates the resonance field enhancement takes place in the vicinity of $\lambda=370$ and 505 nm, respectively.

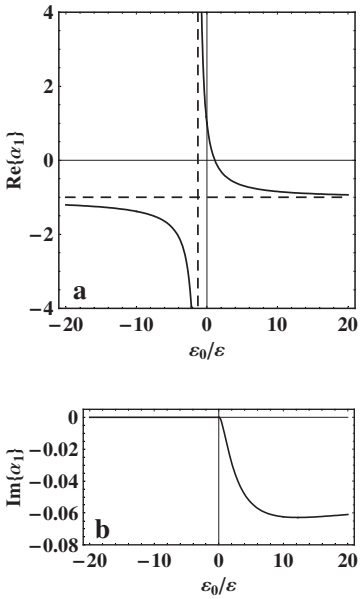


FIG. 6. Real (a) and imaginary (b) parts of the reflection coefficient, $\alpha_1$, as functions of the dielectric constants ratio, $\varepsilon_0/\varepsilon$. Calculations were made at $\omega a\sqrt{\varepsilon}/c=\pi/5$.

Note that in our example the reflection coefficient, $\mathrm{Re}\{\alpha_1\}$, tends to infinity since here we consider a loss-free medium outside a waveguide. If we take into account the imaginary part of the dielectric constant, we simply obtain a strong enhancement in the amplitude of the reflected wave instead of such a singularity. This effect is similar to the plasmon resonance at an interface between the metallic and the dielectric media. The various resonance plasmon-supported effects are intensively discussed now in nano-optics (see, e.g., [34], and references therein). The detailed analysis of the resonance reflection of the evanescent waves from a metallic substrate will be given in a separate paper.

Here it is important to stress that the imaginary part of $\alpha_1$ is equal to zero at $\varepsilon_0/\varepsilon<0$ [see Fig. 6(b)]. This means that the energy flux and the transmission coefficient to the far-field zone are equal to zero, since both these quantities are proportional to the imaginary part of the reflection coefficient, $\mathrm{Im}\{\alpha_1\}$ (see Secs. IV and V).

At the positive values of $\varepsilon_0/\varepsilon$, the imaginary part of $\alpha_1$ is negative that corresponds to the positive energy flux to the far-field zone. The growth of $\mathrm{Re}\{\alpha_1\}$ with a decrease of the $\varepsilon_0/\varepsilon$ ratio means that the transverse component of the electric field, $E_\rho\propto(1+\alpha_1)$, tends to have a loop at the exit plane ($z=0$) for small values of $\varepsilon_0/\varepsilon$. On the contrary, an increase of the $\varepsilon_0/\varepsilon$ ratio leads to a decrease of $\mathrm{Re}\{\alpha_1\}$, such that the amplitude of the transverse component of the electric field tends to have a minimum at the waveguide exit. Thus the dependence of $\alpha_1$ on $\varepsilon_0/\varepsilon$ gives a way to measure the dielectric constants of different samples by detecting the change of

the field characteristics in the near-field probes.

### E. Case of a finite reflectivity of a metal

All results presented above have been obtained for a waveguide with a perfect conductivity of a metallic coating. Here we discuss the validity of our approach in the case of a real metal and investigate the influence of a real dielectric constant on the field behavior in a waveguide with an Al coating. We present some calculations of the reflection coefficient from a nanometric aperture at $\lambda=488$ nm. Our aim is to evaluate the changes in the $\alpha_1$ values, which appear due to a finite dielectric constant of Al.

A schematic diagram of a waveguide with a finite conductivity of its walls is the same as in Fig. 1. However, we describe here the optical properties of a real metal ($a\leq\rho<\infty$, $z<0$) by a dielectric function, $\varepsilon_m$, whose magnitude is equal to $\varepsilon_m=-34.5+i8.5$ for Al at $\lambda=488$ nm. All other notations are the same as in Sec. II, i.e., $\varepsilon$ and $\varepsilon_0$ are the dielectric constants of a waveguide core ($0\leq\rho<a$, $z<0$) and a surrounding medium outside a waveguide ($z>0$), respectively.

In the case of the propagating waves, the studies of the field behavior inside an infinite cylindrical waveguide with a finite dielectric constant of its walls were the subject of Refs. [53,54]. In our case some modifications in the field pattern should be made in order to describe the evanescent wave behavior. Thus in the region of a waveguide core, $0<\rho<a$, we proceed from Eqs. (1)–(3) for the field components, $E_\rho$, $E_z$, and $H_\varphi$. A new point is that the eigenvalue, $\xi=qa$, of the evanescent mode (and, hence, its transverse wave number, $q$) should correspond to a novel boundary value problem [see below Eq. (44)]. This means that in the case of a real metal the $\xi$ value is actually dependent on the specific magnitude of $\varepsilon_m$ and the $a/\lambda$ ratio. As in the preceding sections, we consider here a reflection from a nanometric hole of the evanescent angular symmetrical mode, which corresponds to the $TM_{01}$ mode in a waveguide with perfectly conducting walls.

In the region outside a core, $a<\rho<\infty$, the electric and magnetic fields can now be expressed through the modified Bessel functions

$$\tilde{E}_\rho = CAK_1\left(\chi\frac{\rho}{a}\right)\exp\left(-z\sqrt{q^2-\frac{\omega^2\varepsilon}{c^2}}\right), \tag{39}$$

$$\tilde{E}_z = \frac{-\chi}{\sqrt{q^2-\frac{\omega^2\varepsilon}{c^2}}}CAK_0\left(\chi\frac{\rho}{a}\right)\exp\left(-z\sqrt{q^2-\frac{\omega^2\varepsilon}{c^2}}\right), \tag{40}$$

$$\tilde{H}_\varphi = -i\frac{\omega}{c}\frac{\varepsilon_m}{\sqrt{q^2-\frac{\omega^2\varepsilon}{c^2}}}CAK_1\left(\chi\frac{\rho}{a}\right)\exp\left(-z\sqrt{q^2-\frac{\omega^2\varepsilon}{c^2}}\right). \tag{41}$$

These expressions are written in the approximation of a lossless metal ($-\mathrm{Re}\{\varepsilon_m\}\gg\mathrm{Im}\{\varepsilon_m\}$). So, further we do not take into account the imaginary part of $\varepsilon_m$, that is justified for Al at $\lambda=488$ nm. The normalization constant, $C$, in Eqs. (39)–(41), is the same as in Eqs. (1)–(3), while the magnitude of the $A$ constant should be found from the boundary conditions at an interface ($\rho=a$) of a dielectric core and a real metal. At the same time, the value of $\chi$, which defines the depth of the field penetration into a metallic coating, can be expressed through the eigenvalue $\xi$ according to the wave equation. This yields

$$\xi^2-\frac{\omega^2}{c^2}a^2\varepsilon=-\chi^2-\frac{\omega^2}{c^2}a^2\varepsilon_m. \tag{42}$$

A requirement of matching the fields at a metal-dielectric interface leads to the equations

$$J_1(\xi)\varepsilon = AK_1(\chi)\varepsilon_m,$$

$$J_0(\xi)\xi = -AK_0(\chi)\chi. \tag{43}$$

On excluding the $A$ constant from Eq. (43), we get

$$\xi\frac{J_0(\xi)}{J_1(\xi)} = -\frac{\varepsilon}{\varepsilon_m}\chi\frac{K_0(\chi)}{K_1(\chi)}. \tag{44}$$

Note that a similar equation was obtained in Ref. [54] for the case of guiding waves. In the case of the evanescent waves considered in the present paper the system of Eqs. (42) and (44) enables us to obtain the magnitudes of $\xi$ and $\chi$ for a given value of $\omega/c$.

It is important to stress that the basic points of our theoretical technique, developed for a supercritical waveguide in the preceding sections, remain unchanged if we take into account a finite dielectric constant of metallic walls. Below we briefly describe it, concentrating on modifications which appear in the case of a real metal. In the first stage we evaluate the nonzero field components inside a waveguide core and a metallic coating according to Eqs. (1)–(3) and (39)–(41) and using the $\xi$ and $\chi$ values calculated as noted above. Further, in order to take into account the influence of a nanometric aperture of a truncated waveguide, we must include into our consideration the sum of all possible reflected waves, which appear at a plane interface of a waveguide and a free space ($z=0$, see Fig. 1). Then, we use the first-order approximation according to which we can retain only one of the reflected waves and include it in expressions for the field amplitudes with a factor of $\alpha_1$.

The next step consists of the field construction outside a waveguide using the Fourier-Bessel expansion and of matching the fields at a plane interface of a waveguide and a free space, following the procedure described in Sec. III. It is based on the exact equalizing the $E_\rho$ components on both sides of a plane interface ($z=0$). Then, we apply the requirement for the coincidence of complex flows [see Eq. (55)] instead of a boundary condition for the $H_\varphi$ component (see below Sec. IV for more details).

As a result we obtain a simple equation for the determination of the reflection coefficient and the final expression for $\alpha_1$ can be written as

$$\alpha_1 = \frac{M - I_{11}}{M + I_{11}}. \tag{45}$$

Here the real and imaginary parts of the integral $I_{11} = \mathrm{Re}\{I_{11}\} + i\,\mathrm{Im}\{I_{11}\}$ in Eq. (45) are given by

$$\mathrm{Re}\{I_{11}\} = \int_{\omega/ca\sqrt{\varepsilon_0}}^{\infty} \frac{f(x)xdx}{\sqrt{x^2 - \omega^2 a^2 \varepsilon_0/c^2}}, \tag{46}$$

$$\mathrm{Im}\{I_{11}\} = \int_{0}^{\omega/ca\sqrt{\varepsilon_0}} \frac{f(x)xdx}{\sqrt{\omega^2 a^2 \varepsilon_0/c^2 - x^2}} \tag{47}$$

and the $f(x)$ function in Eqs. (46) and (47) has the form

$$f(x) = \left\{ \frac{1}{x^2 - \xi^2} \frac{1}{J_1(\xi)} [xJ_2(x)J_1(\xi) - \xi J_1(x)J_2(\xi)] - \frac{1}{x^2 + \chi^2} \frac{\varepsilon}{\varepsilon_m} \frac{1}{K_1(\chi)} [xJ_2(x)K_1(\chi) - \chi J_1(x)K_2(\chi)] \right\}^2. \tag{48}$$

The $M$ quantity in Eq. (45) for the reflection coefficient can be written as

$$M = \frac{1}{2\sqrt{\xi^2 - \frac{\omega^2}{c^2} a^2 \varepsilon}} \left\{ \frac{\varepsilon}{\varepsilon_0} \frac{1}{J_1^2(\xi)} [J_1^2(\xi) - J_0(\xi)J_2(\xi)] - \frac{\varepsilon^2}{\varepsilon_0 \varepsilon_m} \frac{1}{K_1^2(\chi)} [K_1^2(\chi) - K_0(\chi)K_2(\chi)] \right\}. \tag{49}$$

Following a technique presented above we have made the calculations of the reflection coefficient, $\alpha_1$, from a nanometric aperture of a waveguide with a glass core ($\varepsilon = 2.25$) and an Al coating ($\mathrm{Re}\{\varepsilon_m\} = -34.5$) at $\lambda = 488$ nm. The dielectric constant of a surrounding medium outside a waveguide was chosen to be equal to $\varepsilon_0 = 1$. The results of these calculations for the real and imaginary parts of $\alpha_1$ are shown in Fig. 7 as functions of $ka$, where $k = \omega\sqrt{\varepsilon_0}/c$. We also display in Fig. 7 the corresponding results obtained for the case of perfectly conducting walls. As follows from a comparison of the results obtained the qualitative behavior of the reflection coefficient versus $ka$ remains the same for real and ideal metals provided that the evanescent mode under investigation does exist inside a waveguide with an Al coating, i.e., at $ka > ka_{\min}^{\mathrm{Al}}$ [where $ka_{\min}^{\mathrm{Al}} = 0.3961$ is a point at which the $\chi$ value in Eqs. (39)–(41) becomes equal to zero]. The corresponding values turn out to be particularly close to each other in the range of $ka_{\min}^{\mathrm{Al}} < ka \lesssim 1$. At $0 < ka < ka_{\min}^{\mathrm{Al}}$ such a mode disappears inside a waveguide with the Al coating, so that the model with a perfect metal does not hold. It is also seen from Fig. 1 that the differences between the cases of real (Al) and ideal metals increase with an increase of the $ka$ value. These differences turn out to be maximal near the point $ka_{\max}^{\mathrm{Al}}$, where $ka_{\max}^{\mathrm{Al}} = \xi_1^{\mathrm{Al}}\sqrt{\varepsilon_0/\varepsilon} = 1.2860$. Starting from $ka > 1.2860$ the evanescent mode is transformed into the propagating one (for an ideal metal this occurs at $ka_{\max}^{\mathrm{ideal}} = \xi_1^{\mathrm{ideal}}\sqrt{\varepsilon_0/\varepsilon} = 1.6032$). On the whole, however, our present calculations indicate that in the case of a lossless metal with sufficiently high negative permittivity a model with a perfectly conducting coating has a sufficiently wide region of validity.

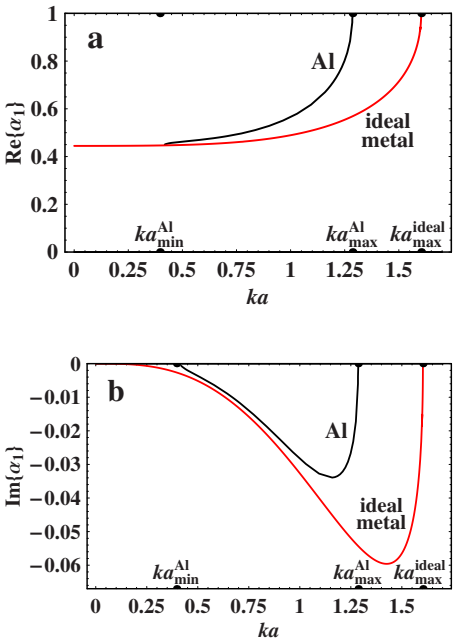


FIG. 7. (Color online) Real and imaginary parts of the amplitude reflection coefficient, $\alpha_1$, as a function of $ka$ ($k = \omega\sqrt{\varepsilon_0}/c$). Calculations were made within the framework of the first-order approximation for the lowest-order transverse-magnetic mode in a waveguide with a glass core ($\varepsilon = 2.25$) and an Al coating ($\mathrm{Re}\{\varepsilon_m\} = -34.5$). The dielectric constant of a free space, $\varepsilon_0$, was taken to be equal to unity.

## IV. COMPLEX FLOW

Now we evaluate a complex flow through a subwavelength-sized exit hole in a waveguide. Our aim is to obtain a relationship between the complex flow, $j$, and the amplitude reflection coefficient, $\alpha_1$. According to the general definition [25,51] a complex flow, $j$, along the $z$ axes through an area $\pi a^2$ is expressed through the $z$ component of the time-averaged complex Poynting vector, $\mathbf{P}$, integrated over this area (see Fig. 1),

$$j = 2\pi \int_0^a P_z \rho d\rho,$$

$$\mathbf{P} = \frac{c}{8\pi}[\mathbf{E} \times \mathbf{H}^*], \tag{50}$$

where $c$ is the speed of light in vacuum. Formula (50) is written for the monochromatic wave with angular independent field components. We deal below with a renormalized complex flow through the exit aperture ($z = 0$),

$$S = \int_0^a [\mathbf{E} \times \mathbf{H}^*]_z \rho d\rho. \tag{51}$$

It corresponds to a free space and differs from the standard definition only by a factor $c/4$. A similar expression for a

complex flow inside a waveguide is given by

$$\tilde{S} = \int_0^a [\tilde{\mathbf{E}} \times \tilde{\mathbf{H}}^*]_z \rho d\rho. \tag{52}$$

To derive the explicit expression for a complex flow inside a waveguide, $\tilde{S}$, at the exit aperture ($z=0$) we proceed from Eqs. (10) and (12) for the electromagnetic fields and use the first-order approximation (when $\alpha_n=0$ for $n\neq 1$). On inserting Eqs. (10) and (12) into Eq. (52), and using Eq. (24), after integration over the $\rho d\rho$ we obtain the following result:

$$\tilde{S} = \int_0^a [\tilde{\mathbf{E}} \times \tilde{\mathbf{H}}^*]_z \rho d\rho = \int_0^a \tilde{E}_\rho(\rho,0)\tilde{H}_\varphi^*(\rho,0)\rho d\rho$$

$$= i\frac{\omega}{c}\varepsilon |C|^2(1+\alpha_1)(1-\alpha_1^*)\frac{a^3 J_1^2(q_1 a)}{2\sqrt{\xi_1^2 - \omega^2 a^2 \varepsilon/c^2}}. \tag{53}$$

To evaluate the complex flow at the exit aperture ($z=0$) outside a waveguide, $S$, we take Eq. (10) for $\tilde{E}_\rho(\rho,0)=E_\rho(\rho,0)$ and Eq. (21) for $H_\varphi(\rho,0)$ in the first-order approximation. Then, integration over the $\rho d\rho$ in Eq. (51) yields

$$S = \int_0^a [\mathbf{E} \times \mathbf{H}^*]_z \rho d\rho$$

$$= \int_0^a E_\rho(\rho,0)H_\varphi^*(\rho,0)\rho d\rho = i\frac{\omega}{c}a^3\varepsilon_0 |C|^2 |1+\alpha_1|^2 J_1^2(q_1 a) I_{11}^*. \tag{54}$$

Further we use Eqs. (53) and (54) to clarify the meaning of our basic equation (30). It is seen that on dividing Eq. (54) for $S$ by a factor $-i\frac{\omega}{c}CC^*(1+\alpha_1^*)J_1^2(q_1 a)a^2/2$ and using complex conjugation, it coincides with the left-hand side of Eq. (30). At the same time, on dividing Eq. (53) for $\tilde{S}$ by the same factor and using complex conjugation, it coincides with the right-hand side of Eq. (30). Now it is clear that the basic equation (30) can be interpreted as the equality of the outer complex flow and the inner one, i.e.,

$$\tilde{S} = S. \tag{55}$$

This form of basic equation (30) clarifies the entity of our approach to the field calculations. The matter is that the results of calculations would be the same if we used, from the beginning, the condition of the coincidence of complex flows instead of the equalization of the magnetic fields $H_\varphi$ and $\tilde{H}_\varphi$ at each point of the exit aperture. Note that here it is necessary to consider just a complex flow since it provides information on the phase relations between the $E_\rho$ and $H_\varphi$ components. As a result, Eq. (55) for complex flows $\tilde{S}$ and $S$ enables us to find a complex reflection coefficient, $\alpha_1$.

It is worthwhile to remember here that the standard boundary condition consists of the coincidence of both the electric and magnetic tangential fields at an interface of the two media. For a simple geometry (when the $E/H$ ratio does not depend on the transverse coordinate) such a condition is equivalent (see [25,51]) to the requirement of the conservation of the $E_{\text{tang}}/H_{\text{tang}}$ ratio combined with the conservation of the tangential component of the electric field, $E_{\text{tang}}$, at that interface. For more complicated cases, we propose to introduce the ratio of the following integrals:

$$\frac{W_\rho}{S^*} = \frac{\int_0^a E_\rho^*(\rho,0)E_\rho(\rho,0)\rho d\rho}{\int_0^a E_\rho^*(\rho,0)H_\varphi(\rho,0)\rho d\rho} = Z_a, \tag{56}$$

instead of the $E_\rho/H_\varphi$ ratio. Here $W_\rho$ is the square of the tangential component of the electric field integrated over the aperture:

$$W_\rho = \int_0^a E_\rho^*(\rho,0)E_\rho(\rho,0)\rho d\rho. \tag{57}$$

The quantity $Z_a$, introduced by Eq. (56), plays the role of the impedance of the exit aperture, which couples the waveguide to the free space. Such a quantity, $Z_a$, allows us to get an appropriate solution of the boundary problem in more complicated cases, when the $E_\rho/H_\varphi$ ratio does vary in the transverse direction.

The results of the previous sections definitely demonstrate that the reflection from the interface of a waveguide and a free space can be completely determined by the quantities $Z_a$ and $Z_\varepsilon$, where

$$Z_\varepsilon = i\frac{\sqrt{q_1^2 - \omega^2\varepsilon/c^2}}{(\omega\varepsilon/c)} \tag{58}$$

is the impedance for the evanescent mode of the waveguide with a dielectric constant, $\varepsilon$, of its core.

As to the $W_\rho$ quantity in Eq. (56), one should mention that in the first-order approximation its value can be evaluated with the use of Eq. (10), taking into account Eq. (24). The final result is given by

$$W_\rho = |C|^2|1+\alpha_1|^2\frac{a^2}{2}J_1^2(q_1 a), \tag{59}$$

where $J_1^2(q_1 a)=0.2695$, and $\xi_1=q_1 a=2.4048$ is the first zero of the Bessel function $J_0(\xi_1)=0$.

The relationships between this value and the complex flow at an interface between a waveguide and a free space ($\tilde{S}=S$) can be derived with the help of Eqs. (53), (54), and (59). This yields

$$\frac{\tilde{S}^*}{W_\rho} = -\frac{i\omega}{c}\frac{\varepsilon}{\sqrt{q_1^2 - \omega^2\varepsilon/c^2}}\left(\frac{1-\alpha_1}{1+\alpha_1}\right), \tag{60}$$

$$\frac{S^*}{W_\rho} = -2i\frac{\omega a \varepsilon_0}{c}I_{11} = \frac{1}{Z_a}. \tag{61}$$

In accordance with Eq. (56), formula (61) gives an explicit expression for the impedance of the exit aperture. It is also worthwhile to point out that formula (60) being combined with Eqs. (56) and (58) provides some new form of equation for the reflection coefficient

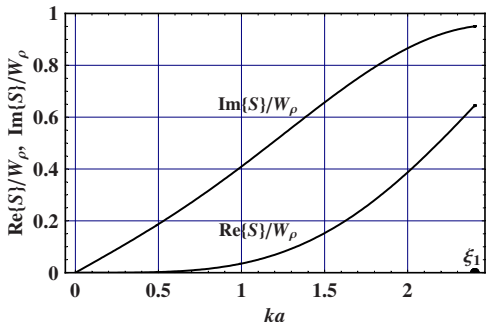


FIG. 8. (Color online) Ratios of the real and imaginary parts of a complex flow, $S$ (54), to the integral energy density, $W_\rho$, of the transverse component of the electric field (57). Calculations were made for the $TM_{01}$ mode at $\varepsilon=\varepsilon_0=1$.

$$\frac{Z_\varepsilon}{Z_a}=\frac{1-\alpha_1}{1+\alpha_1}. \tag{62}$$

In particular, Eq. (62) allows us to express the reflection coefficient, $\alpha_1$, in terms of the ratio of impedances, $Z_\varepsilon/Z_a$.

Using Eq. (61) the real and imaginary parts of the $S/W_\rho$ ratio can be written as

$$\frac{\mathrm{Re}\{S\}}{W_\rho}=\left(\frac{2\omega a\varepsilon_0}{c}\right)\mathrm{Im}\{I_{11}\}, \tag{63}$$

$$\frac{\mathrm{Im}\{S\}}{W_\rho}=\left(\frac{2\omega a\varepsilon_0}{c}\right)\mathrm{Re}\{I_{11}\}, \tag{64}$$

where $\mathrm{Re}\{I_{11}\}$ and $\mathrm{Im}\{I_{11}\}$ are given by Eqs. (26) and (27). In accordance with Eq. (28), the ratio of the real part of a complex flow to the integral energy density of the transverse electric field takes a particularly simple form in the asymptotic region of small $ka$ values,

$$\frac{\mathrm{Re}\{S\}}{W_\rho}=\frac{4\sqrt{\varepsilon_0}}{3\xi_1^4}(ka)^4=0.039\ 87\sqrt{\varepsilon_0}(ka)^4. \tag{65}$$

For the $TM_{01}$ field mode under investigation the dependencies of the real and imaginary parts of the ratio $S/W_\rho$ on the $ka$ value are shown in Fig. 8.

Note that a complex reflection coefficient, $\alpha_1$, of the evanescent wave from a subwavelength hole affects different components of the electromagnetic energy density at the waveguide exit in different ways. As is evident from Eq. (59), the transverse component of the electric field square, $W_\rho$, in Eqs. (60)–(65) is proportional to the factor $|1+\alpha_1|^2$. On the contrary, the longitudinal electric field square, $W_z$, and the transverse-magnetic field square, $W_\varphi$, turn out to be proportional to $|1-\alpha_1|^2$. This directly proceeds from the following expressions:

$$W_z=\int_0^a E_z^*(\rho,0)E_z(\rho,0)\rho d\rho=\frac{\varepsilon a^2|C|^2|1-\alpha_1|^2(q_1a)^2}{2(q_1^2a^2-\omega^2a^2\varepsilon/c^2)}J_1^2(q_1a), \tag{66}$$

$$W_\varphi=\int_0^a H_\varphi^*(\rho,0)H_\varphi(\rho,0)\rho d\rho=\left(\frac{\omega a\sqrt{\varepsilon}}{c}\right)^2\frac{\varepsilon a^2|C|^2|1-\alpha_1|^2}{2(q_1^2a^2-\omega^2a^2\varepsilon/c^2)}J_1^2(q_1a), \tag{67}$$

obtained using the first-order approximation for the electric and magnetic fields (11) and (12).

## V. FAR-FIELD TRANSMISSION COEFFICIENT

The basic formulas, derived for a complex flow in the preceding section, enable us to evaluate the transmission coefficient to the far-field zone. The far-field transmission coefficient is a quantity, which is commonly used for the estimation of the efficiency of the near-field optical probes. Such a coefficient was first introduced by Bethe and Bouwkamp [22,23] for the leakage of the plane electromagnetic wave through a small hole in a perfectly conducting metallic screen. It was determined through the ratio of the energy fluxes. According to [22,23] it is equal to the flux, appearing behind the aperture, divided by the incident flux (which would exist when it was not affected by the presence of the opaque screen and the aperture):

$$T=\frac{\int\int Pd\sigma}{\int\int P^{\mathrm{inc}}d\sigma}\equiv\frac{\mathrm{Re}\left\{\int\int E_{\mathrm{tang}}H_{\mathrm{tang}}^*\rho d\rho d\varphi\right\}}{\mathrm{Re}\left\{\int\int E_{\mathrm{tang}}^{\mathrm{inc}}(H_{\mathrm{tang}}^{\mathrm{inc}})^*\rho d\rho d\varphi\right\}}. \tag{68}$$

This standard definition of the transmission coefficient is not acceptable, however, for our consideration. The matter is that, for the supercritical waveguide the unperturbed field does not bear the energy flux. Formally, the nonzero flux appears here only upon account of perturbation, associated with the presence of the subwavelength exit hole. Therefore it is impossible for us to directly use Eq. (68). This expression can be easily transformed in order to obtain a somewhat modified definition of the transmission coefficient. We should merely take into account that the authors of Refs. [22,23] dealt with the initially plane wave, which was sent onto the screen. For the plane wave, formula (68) can be interpreted in some other terms. As the amplitudes $E_{\mathrm{tang}}^{\mathrm{inc}}$ and $H_{\mathrm{tang}}^{\mathrm{inc}}$ of the plane wave are equal to each other, we can substitute $E_{\mathrm{tang}}^{\mathrm{inc}}$ instead of $H_{\mathrm{tang}}^{\mathrm{inc}}$ in the denominator of the ratio (68) and reduce it to the form

$$T=\frac{\mathrm{Re}\left\{\int\int E_{\mathrm{tang}}H_{\mathrm{tang}}^*\rho d\rho d\varphi\right\}}{\int\int E_{\mathrm{tang}}^{\mathrm{inc}}(E_{\mathrm{tang}}^{\mathrm{inc}})^*\rho d\rho d\varphi}. \tag{69}$$

This type of representation of the transmission coefficient is perfectly suitable for our consideration. Starting from this formula we can derive the expression for the transmission coefficient in terms of the quantities obtained in the previous sections. To this end, one should remember that in the first-

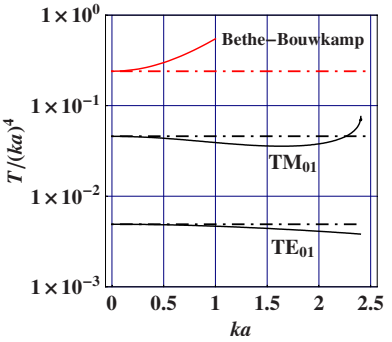


FIG. 9. (Color online) Far-field transmission coefficient, $T$, divided by a factor $(ka)^4$. The full curves are the results for the $TM_{01}$ and $TE_{01}$ modes, obtained by the general equations (63), (70), (81), and (82). The dashed curves are the corresponding results obtained by the asymptotic ($ka \ll 1$) formulas (65) and (83). The upper full curve is the Bethe-Bouwkamp result (71) for transmission of a plane wave through a small hole in a perfectly conducting screen. The upper dashed curve is the contribution of the first term in Eq. (71). All calculations were made for $\varepsilon_0=1$.

order approximation the resulting electric field at the waveguide exit differs from the unperturbed transverse field by a factor of $(1+\alpha_1)$. It is also necessary to take into account that for the $TM_{01}$ mode the field components do not depend on the angular coordinate $\varphi$. Then, a comparison of Eqs. (69) and (63) shows that the final expression for the transmission coefficient in our problem should be written as

$$T = |1+\alpha_1|^2 \frac{\mathrm{Re}\left\{\int\int E_\rho H_\varphi^* \rho d\rho\right\}}{\int\int E_\rho E_\rho^* \rho d\rho} \equiv \frac{\mathrm{Re}\{S\}}{W_\rho}|1+\alpha_1|^2 = |1+\alpha_1|^2 \frac{2\omega a \varepsilon_0}{c}\mathrm{Im}\{I_{11}\}. \quad (70)$$

The results of our calculations of the far-field transmission coefficient (70), divided by a factor $(ka)^4$, are shown in Fig. 9 versus the $ka$ value (where $k=\omega\sqrt{\varepsilon_0}/c$). These calculations have been performed by using the general expressions (70) and (63) for the transverse-magnetic mode, $TM_{01}$. As is evident from the figure, the asymptotic behavior of the $T/(ka)^4$ quantity at small values of $ka$ is in agreement with Eqs. (70) and (65) of Sec. IV. In Fig. 9 we also display the corresponding results for the transverse-electric mode, $TE_{01}$. One can see that the transmission coefficient for the $TM_{01}$ mode turns out to be 8.12 times greater than that for the $TE_{01}$ mode. Thus the transmission coefficient is strongly dependent on the type of the incident field mode.

It is also interesting to compare our results with those obtained using the Bethe and Bouwkamp formula [22,23],

$$T = \frac{\mathrm{Re}\{S\}}{W^{\mathrm{inc}}} = \frac{64}{27\pi^2}(ka)^4\left[1+\frac{22}{25}(ka)^2+\frac{7312}{18375}(ka)^4+\cdots\right]. \quad (71)$$

The calculations show that this formula gives the $T$ value that exceeds the corresponding results for the $TM_{01}$ and $TE_{01}$ modes for 6.02 and 48.93 times, respectively.

## VI. EXTENSION TO THE CASE OF THE TRANSVERSE-ELECTRIC FIELD MODE, $TE_{01}$

Although all results presented above have been obtained for the lowest-order transverse-magnetic mode, $TM_{01}$, our technique assumes an extension to the case of other field configurations. For the angular-symmetrical transverse-electric mode, $TE_{01}$, this can be done with minimal modifications of the approach and the form of final results. In this case instead of Eqs. (7)–(9) one should proceed from the following basic expressions for the nonzero field components inside a waveguide

$$\tilde{E}_\varphi = CJ_1(q\rho)\left[\exp\left(-z\sqrt{q^2-\frac{\omega^2\varepsilon}{c^2}}\right)+\alpha\exp\left(z\sqrt{q^2-\frac{\omega^2\varepsilon}{c^2}}\right)\right], \quad (72)$$

$$\tilde{H}_\rho = \frac{C}{(i\omega/c)}\sqrt{q^2-\frac{\omega^2\varepsilon}{c^2}}J_1(q\rho)\left[\exp\left(-z\sqrt{q^2-\frac{\omega^2\varepsilon}{c^2}}\right)-\alpha\exp\left(z\sqrt{q^2-\frac{\omega^2\varepsilon}{c^2}}\right)\right], \quad (73)$$

$$\tilde{H}_z = \frac{C}{(i\omega/c)}qJ_0(q\rho)\left[\exp\left(-z\sqrt{q^2-\frac{\omega^2\varepsilon}{c^2}}\right)-\alpha\exp\left(z\sqrt{q^2-\frac{\omega^2\varepsilon}{c^2}}\right)\right]. \quad (74)$$

Here $q=\xi_1^{(\mathrm{TE})}/a$, $\xi_1^{(\mathrm{TE})}=3.832$ is the first root of equation $J_1(x)=0$, and the amplitude reflection coefficient, $\alpha\equiv\alpha_1$, obeys the equation

$$\frac{1-\alpha}{1+\alpha}=G, \quad G=\frac{(\xi_1^{(\mathrm{TE})})^2 2I_{11}}{\sqrt{(\xi_1^{(\mathrm{TE})})^2-\frac{\omega^2a^2\varepsilon}{c^2}}}. \quad (75)$$

Note that for the $TE_{01}$ mode the form of expression for the $G$ quantity in Eq. (75) differs from the corresponding Eq. (32) for the $TM_{01}$ mode. The real and imaginary parts of the integral, $I_{11}$, in Eq. (75) are given by

$$\mathrm{Re}\{I_{11}\}=\int_{\omega a/c\sqrt{\varepsilon_0}}^{\infty}\sqrt{x^2-\frac{\omega^2\varepsilon_0}{c^2}a^2}\frac{J_1^2(x)xdx}{[(\xi_1^{(\mathrm{TE})})^2-x^2]^2}, \quad (76)$$

$$\mathrm{Im}\{I_{11}\} = -\int_0^{\omega a/c\sqrt{\varepsilon_0}} \sqrt{\frac{\omega^2\varepsilon_0}{c^2}a^2 - x^2}\,\frac{J_1^2(x)x dx}{[(\xi_1^{(\mathrm{TE})})^2 - x^2]^2}. \tag{77}$$

Below we present the resulting expressions for the electric field square integrated over the aperture cross section, $W_\varphi$, and for the complex flow, $S$, associated with the $\mathrm{TE}_{01}$ mode,

$$W_\varphi = |C|^2|1+\alpha|^2\frac{a^2}{2}J_0^2(\xi_1^{(\mathrm{TE})}), \tag{78}$$

$$S = -\frac{iW_\varphi}{(\omega a/c)}\left(\frac{1-\alpha^*}{1+\alpha^*}\right)\sqrt{(\xi_1^{(\mathrm{TE})})^2 - \frac{\omega^2 a^2\varepsilon^*}{c^2}}. \tag{79}$$

The ratio of $S/W_\varphi$ can also be written as

$$\frac{S}{W_\varphi} = -\frac{2i(\xi_1^{(\mathrm{TE})})^2 I_{11}^*}{(\omega a/c)}. \tag{80}$$

For the energy flux and the resulting transmission coefficient, we have

$$\frac{\mathrm{Re}\{S\}}{W_\varphi} = -\frac{2(\xi_1^{(\mathrm{TE})})^2}{\omega a/c}\mathrm{Im}\{I_{11}\}, \tag{81}$$

$$T = |1+\alpha|^2\frac{\mathrm{Re}\left\{\int\int E_\varphi H_\rho^* \rho d\rho\right\}}{\int\int E_\varphi E_\varphi^* \rho d\rho} \equiv \frac{\mathrm{Re}\{S\}}{W_\varphi}|1+\alpha|^2. \tag{82}$$

At small $ka$ values ($ka = \omega a\sqrt{\varepsilon_0}/c$) the expression (81) can be written as

$$\frac{\mathrm{Re}\{S\}}{W_\varphi} = \frac{\sqrt{\varepsilon_0}}{15(\xi_1^{(\mathrm{TE})})^2}(ka)^4 = 0.004\,908\sqrt{\varepsilon_0}(ka)^4. \tag{83}$$

A comparison of Eqs. (78)–(81) with (59)–(61) demonstrates some common features in the description of the $\mathrm{TE}_{01}$ and $\mathrm{TM}_{01}$ modes in a truncated waveguide. We note, however, that the transmission efficiency for the $\mathrm{TE}_{01}$ wave turns out to be much lower than that for the $\mathrm{TM}_{01}$ wave, as it was already shown in Fig. 9.

## VII. CONCLUSIONS

(1) To summarize, we have developed a theoretical approach for the calculation of the spatial structure of the evanescent electromagnetic fields in a truncated waveguide and in a free space behind its exit aperture. The approach is based on a rigorous technique for matching the superposition of the waveguide modes with the field outside a waveguide, represented by the Fourier-Bessel integrals over the transverse wave numbers. It was shown that for a supercritical waveguide the initial field is predominantly transformed into the mode with the identical transverse structure and the inverse dependence on the longitudinal coordinate.

(2) We have introduced the amplitude reflection coefficient for the evanescent wave, which initially impinges onto the aperture. It was expressed as a function of the waveguide radius, the radiation wavelength, and the dielectric constants of the waveguide core and the free space. It was shown that the reflection coefficient is particularly small when there is no discontinuity in the dielectric function at the exit aperture. Then, the field of a truncated waveguide does not appreciably differ from the unperturbed field inside a waveguide of an infinite length. The jump in the dielectric function significantly affects the amplitude of the reflected wave and modifies the field amplitude in the vicinity of the exit hole. In this case, the field at an interface of a truncated waveguide and a free space is close to the field in an infinite waveguide at an interface of the two regions with different refractive indices.

(3) The growth in the ratio of the positive dielectric constant of the waveguide core, $\varepsilon$, to the positive dielectric constant of the external matter, $\varepsilon_0$, leads to an increase of the reflection coefficient, $\alpha_1$. It can approach unity at large values of $\varepsilon/\varepsilon_0$. This yields a fourfold increase in the energy density, $w_\rho \propto |1+\alpha_1|^2$, of the transverse component of the electric field as compared to the case of the unperturbed waveguide of an infinite length. Such an increase in the electric field amplitude at the exit aperture clearly demonstrates the advantage in the use of the near-field probes with high values of the core dielectric constant. Thus it affects the transmission coefficient of an optical probe in the same direction as a decrease of the damping of the evanescent waves in the supercritical tapered waveguide (see, e.g., Refs. [15–18]).

(4) It was demonstrated that in the case of a metallic substrate at the waveguide exit there is a strong resonance enhancement in the amplitude of the reflected wave. This enhancement in the reflection coefficient and in the amplitude of the tangential component of the electric field is a manifestation of the plasmon-supported effects. Note that the strong dependence of the field amplitude at the waveguide exit on the permittivity of an environment provides a tool for the measurement of the dielectric constants of external objects.

(5) We have calculated the far-field transmission coefficient for the $\mathrm{TM}_{01}$ and $\mathrm{TE}_{01}$ modes. It was shown that such a quantity is strongly affected by the type of the initial waveguide mode. The transmission coefficient for the $\mathrm{TM}_{01}$ mode turns out to be for about one order of magnitude greater than that for the $\mathrm{TE}_{01}$ mode. Furthermore, the values of such transmission coefficients differ drastically from the case of the leakage of the linearly polarized plane wave through a small hole in the thin metallic screen.

(6) On the basis of the theory developed we have evaluated a complex flow at the waveguide exit. It was shown that the continuity of the complex flow provides a suitable boundary condition for the construction of an approximate solution of a boundary problem. The results obtained for the fields characteristics (e.g., for the reflection coefficient) have been reformulated in terms of the impedance for the evanescent waves. To this end, we have introduced the impedance associated with the exit aperture at an interface of a waveguide and a free space.

(7) Although our consideration has been primarily performed for the lowest-order transverse-magnetic mode, $\mathrm{TM}_{01}$, we outlined a way for its extension to the case of the

evanescent transverse-electric mode, $TE_{01}$. Moreover, the theory assumes further generalization to the case of the tapered waveguides, which are of special interest for the near-field optical microscopy.

(8) Finally, we note that despite that our approach was developed for a waveguide with perfectly conducting walls it is a basis for the next generalization to the case of a finite dielectric constant of its metallic coating. It was demonstrated by numerical calculations for an Al coating of a waveguide with a glass core at $\lambda = 488$ nm. The results obtained allow us to conclude that in the case of a lossless metal with a high negative permittivity a model with perfectly conducting walls has a sufficiently wide range of validity. One can expect, however, that some resonance plasmon-supported phenomena in light transmission through an exit aperture would become important for noble metallic coating of a supercritical waveguide similar to the case of nanoholes in noble metal films.

## ACKNOWLEDGMENTS

This work was supported by the Programmes "Optical Spectroscopy and Frequency Standards" and "Coherent Optical Emission of Semiconductor Compounds and Structures" of the Division of Physical Sciences of the Russian Academy of Sciences and by the Russian Foundation for Basic Research (Projects No. 06-02-17089, No. 07-02-00873, and No. 07-02-00656).

[1] D. W. Pohl, Philos. Trans. R. Soc. London, Ser. B **362**, 701 (2004).
[2] B. Hecht, B. Sick, U. P. Wild, V. Deckert, R. Zenobi, O. J. F. Martin, and D. W. Pohl, J. Chem. Phys. **112**, 7761 (2000).
[3] T. Dziomba, H. U. Danzebrink, C. Lehrer, L. Frey, T. Sulzbach, and O. Ohlsson, J. Microsc. **202**, 22 (2001).
[4] A. Naber, D. Molenda, U. C. Fischer, H.-J. Maas, C. Höppener, N. Lu, and H. Fuchs, Phys. Rev. Lett. **89**, 210801 (2002).
[5] T. Thio, K. M. Pellerin, R. A. Linke, H. J. Lezec, and T. W. Ebbesen, Opt. Lett. **26**, 1972 (2001).
[6] H. J. Lezec, A. Degiron, E. Devaux, R. A. Linke, L. Martín-Moreno, F. J. García-Vidal, and T. W. Ebbesen, Science **297**, 820 (2002).
[7] T. W. Ebbesen, H. J. Lezec, H. F. Ghaemi, T. Thio, and P. A. Wollf, Nature (London) **391**, 667 (1998).
[8] N. Bonod, S. Enoch, L. Li, E. Popov, and M. Nevière, Opt. Express **11**, 482 (2003).
[9] L. Novotny, D. W. Pohl, and P. Regli, J. Opt. Soc. Am. A **11**, 1768 (1994).
[10] L. Novotny, D. W. Pohl, and B. Hecht, Opt. Lett. **20**, 970 (1995); Ultramicroscopy **61**, 1 (1995).
[11] A. Castiaux, C. Girard, A. Dereux, O. J. F. Martin, and J.-P. Vigneron, Phys. Rev. E **54**, 5752 (1996).
[12] C. Girard, C. Joachim, and S. Gauthier, Rep. Prog. Phys. **63**, 893 (2000).
[13] T. I. Kuznetsova and V. S. Lebedev, Kvantovaya Elektron. (Moscow) **33**, 931 (2003) [Quantum Electron. **33**, 931 (2003)]; J. Russ. Laser Res. **24**, 458 (2003).
[14] T. I. Kuznetsova, V. S. Lebedev, and A. M. Tsvelik, J. Opt. A, Pure Appl. Opt. **6**, 338 (2004).
[15] T. I. Kuznetsova and V. S. Lebedev, Pis'ma Zh. Eksp. Teor. Fiz. **79**, 70 (2004) [JETP Lett. **79**, 62 (2004)].
[16] T. I. Kuznetsova and V. S. Lebedev, Kvantovaya Elektron. (Moscow) **34**, 361 (2004) [Quantum Electron. **34**, 361 (2004)].
[17] T. I. Kuznetsova and V. S. Lebedev, Phys. Rev. B **70**, 035107 (2004).
[18] V. S. Lebedev, T. I. Kuznetsova, and A. G. Vitukhnovsky, Dokl. Akad. Nauk **410**, 749 (2006) [Dokl. Phys. **51**, 542 (2006)].
[19] H. Furukawa and S. Kawata, Opt. Commun. **132**, 170 (1996).
[20] H. Nakamura, T. Sato, H. Kambe, K. Sawada, and T. Saiki, J. Microsc. **202**, 50 (2001).
[21] S. Mitsugi, Y. J. Kim, and K. Goto, Opt. Rev. **8**, 120 (2001).
[22] H. A. Bethe, Phys. Rev. **66**, 163 (1944).
[23] C. J. Bouwkamp, Philips. Res. Rep. **5**, 321 (1950); Rep. Prog. Phys. **17**, 35 (1954).
[24] L. Rayleigh, Philos. Mag. **44**, 28 (1897).
[25] L. D. Landau, E. M. Lifshitz, and L. P. Pitaevskii, *Electrodynamics of Continuous Media*, 2nd ed. (Pergamon, Oxford, 1993).
[26] A. Roberts, J. Appl. Phys. **70**, 4045 (1991).
[27] A. Drezet, J. C. Woehl, and S. Huant, Phys. Rev. E **65**, 046611 (2002).
[28] F. J. García de Abajo, Opt. Express **10**, 1475 (2002).
[29] L. Alvarez, A. Sauceda, and M. Xiao, Opt. Commun. **219**, 9 (2003).
[30] H. J. Lezec and T. Thio, Opt. Express **12**, 3629 (2004).
[31] J. Olkkonen, K. Kataja, and D. G. Howe, Opt. Express **13**, 6980 (2005).
[32] F. J. García-Vidal, E. Moreno, J. A. Porto, and L. Martín-Moreno, Phys. Rev. Lett. **95**, 103901 (2005).
[33] K. J. Webb and J. Li, Phys. Rev. B **73**, 033401 (2006).
[34] W. L. Barnes, J. Opt. A, Pure Appl. Opt. **8**, S87 (2006).
[35] F. J. García de Abajo, Rev. Mod. Phys. **79**, 1267 (2007).
[36] F. J. García-Vidal and L. Martín-Moreno, Phys. Rev. B **66**, 155412 (2002).
[37] L. Martín-Moreno, F. J. García-Vidal, H. J. Lezec, A. Degiron, and T. W. Ebbesen, Phys. Rev. Lett. **90**, 167401 (2003).
[38] A. Degiron and T. W. Ebbesen, Opt. Express **12**, 3694 (2004).
[39] H. F. Ghaemi, T. Thio, D. E. Grupp, T. W. Ebbesen, and H. J. Lezec, Phys. Rev. B **58**, 6779 (1998).
[40] E. Popov, M. Nevière, S. Enoch, and R. Reinisch, Phys. Rev. B **62**, 16100 (2000).
[41] L. Martín-Moreno, F. J. García-Vidal, H. J. Lezec, K. M. Pellerin, T. Thio, J. B. Pendry, and T. W. Ebbesen, Phys. Rev. Lett. **86**, 1114 (2001).
[42] R. Wannemacher, Opt. Commun. **195**, 107 (2001).
[43] M. Sarrazin, J.-P. Vigneron, and J.-M. Vigoureux, Phys. Rev. B **67**, 085415 (2003).
[44] A. Degiron, H. J. Lezec, N. Yamamoto, and T. W. Ebbesen,

Opt. Commun. **239**, 61 (2004).
[45] L. Yin, V. K. Vlasko-Vlasov, A. Rydh, J. Pearson, U. Welp, S.-H. Chang, S. K. Gray, G. C. Schatz, D. B. Brown, and C. W. Kimball, Appl. Phys. Lett. **85**, 467 (2004).
[46] S.-H. Chang, S. K. Gray, and G. C. Schatz, Opt. Express **13**, 3150 (2005).
[47] T. Rindzevicius, Y. Alaverdyan, B. Sepulveda, T. Pakizeh, M. Kall, R. Hillenbrand, J. Aizpurua, and F. J. García de Abajo, J. Phys. Chem. C **111**, 1207 (2007).
[48] K. L. Shuford, S. K. Gray, M. A. Ratner, and G. C. Schatz, Chem. Phys. Lett. **435**, 123 (2007).
[49] L. A. Vaynshteyn, *Diffraction of the Electromagnetic and Acoustic Waves at the Open End of a Waveguide* (Sovetskoe Radio, Moscow, 1953).
[50] L. A. Vaynshteyn, *Electromagnetic Waves* (Radio i Svyaz, Moscow, 1988) (in Russian).
[51] J. D. Jackson, *Classical Electrodynamics* (Wiley, New York, 1999).
[52] P. B. Johnson and R. W. Christy, Phys. Rev. B **6**, 4370 (1972).
[53] L. Novotny and C. Hafner, Phys. Rev. E **50**, 4094 (1994).
[54] B. Prade and J. Y. Vinet, J. Lightwave Technol. **12**, 6 (1994).